



Pure pompon structured Co–Mo alloy electro-deposited from ethylene glycol solution and used as electrocatalysts for hydrogen evolution reaction

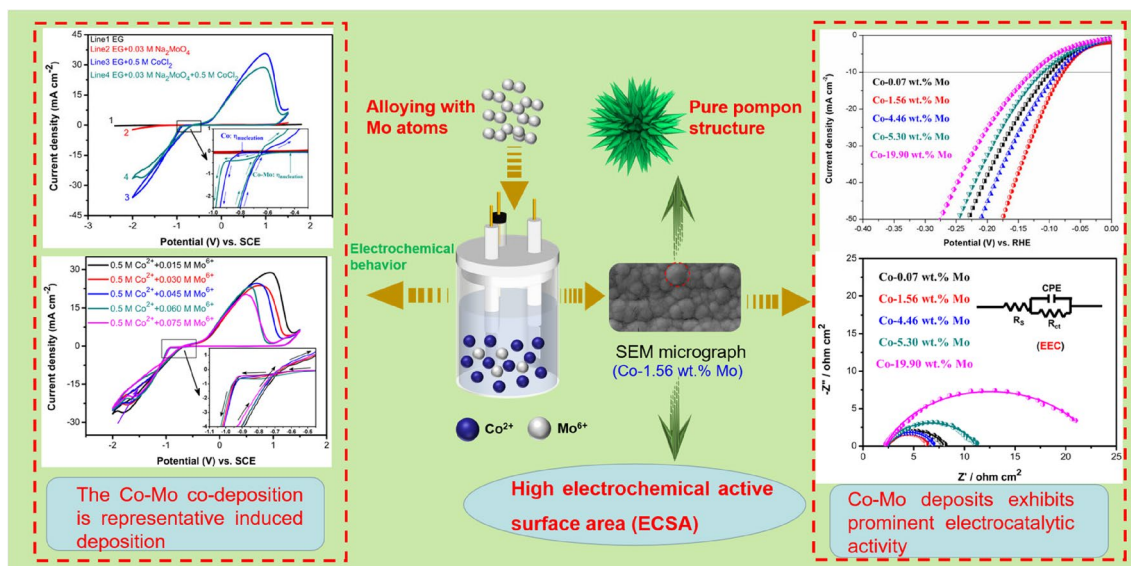
Xinkuai He¹ · Ruqing Guo¹ · Zhousi Hu¹ · Qingtian Zou¹ · Jingjing Yang¹ · Luye Wu¹

Received: 29 December 2022 / Accepted: 12 May 2023 / Published online: 25 May 2023
© The Author(s), under exclusive licence to Springer Nature B.V. 2023

Abstract

The co-deposition behavior of Co(II) and Mo(VI) and Co–Mo electro-crystallization mechanism in ethylene glycol (EG) are recorded using cyclic voltammetry and chronoamperometry. These results indicate that the Co–Mo co-deposition is representative induced deposition; Co(II) species can facilitate Co–Mo co-deposition, inversely, Mo(VI) species can inhibit Co(II) reduction and the effect can be enhanced as Mo(VI) concentration increases. Additionally, Co–Mo co-deposition in EG takes place through an instantaneous nucleation and diffusion-controlled three-dimensional growth mechanism. Co–Mo deposits with various Mo contents and different microstructures can be obtained from the EG solution. SEM micrographs present that the Co–Mo deposits with 1.56 wt% Mo present a pure pompon microstructure. Benefiting from the composition engineering by alloying with Mo, as well as the simultaneous presence of a suitable pompon structure, Co–Mo deposits with 1.56 wt% exhibits prominent electrocatalytic durability and activity with a η_{10} of 84 mV for HER in a 1.0 M KOH.

Graphical abstract



Keywords Co–Mo alloy · Electrodeposition · Ethylene glycol · Electrocatalytic activity

✉ Luye Wu
lyxk999@163.com

¹ School of Packaging and Materials Engineering, Hunan University of Technology, 412007 Zhuzhou, People's Republic of China

1 Introduction

Nowadays, our society is clearly marked by concern about the environmental problem. More and more people are conscious of the fact that excessive consumption of traditional fossil fuel sources such as natural gas, oil, and coal not only gives rise to a diminution in reserves, but also adversely impacts the environment, increasing greenhouse effect or affecting the global climate and resulting in human health risks [1–3]. In order to lower the use of these traditional non-renewable fossil fuels, there is an incentive to develop and employ more and more renewable, sustainable, and clean energy technologies including solar energy, tides energy, wind energy, hydrogen-fueled, and biomass technologies [4–6]. The production of hydrogen based on electrolysis of water can be employed as a potential and energetic alternative due to the fact that hydrogen presents these advantages of being pollution-free, high-energy-density and zero carbon dioxide emissions and the technology can obtain high purity hydrogen [7–19]. However, at present, preparing hydrogen gas from electrolysis is relatively expensive principally due to the use of noble-metal electrocatalysts [20], thus, in order to minimize hydrogen production cost, it has been quite urgent to develop some cheap and high-performance catalysts with low overpotential, high electronic conductivity, good charge transfer kinetics, and long-term stability for hydrogen evolution reaction (HER) and then they can be employed in the practical hydrogen production.

In recent decades, non-noble transition metals catalysts including metal nitrides [16, 21], metal sulfides [17, 22], metal selenides [15, 23], and transition-metal alloys [8, 10–12, 24] had been successfully prepared and exhibited much absorbing consequence. Among these catalysts, Co–Mo alloy and its composite materials are important and promising electrocatalysts for HER due to the fact that these electrode materials exhibit many outstanding properties such as long-term electrochemical stability, good electrical conductivity, high corrosion resistance, outstanding catalytic activity, and low overpotential for the HER [8–12, 15, 19]. These properties can be attributed to the electronic configuration [8, 12, 13] or modification of the crystalline structure when Mo is added into the structure of the iron group Co element [8], and then an outstanding synergistic effect can be obtained by the alloying of hyper d-electronic phase Co, which is the primary source of catalytic activity, and hypo d-electronic phase Mo, who can increase corrosion resistance, mechanical strength, and catalytic activity. It is worth noting that the catalytic activity normally originates from the high free energy on the metastable electrode surface [8, 25].

At present, Co–Mo alloys and its composite materials have been prepared mainly from aqueous solutions [8, 9, 12, 13, 26–31]. For instance, Co–Mo and Co–Mo–C alloys

had been successfully prepared by ŹABIŃSKI et al. from aqueous solution baths containing cobalt sulfate, ammonium molybdate, sodium citrate, sodium dodecylsulphate, saccharin, and arginine (being a source of carbon in the Co–Mo–C alloy) and they found the two alloys exhibited excellent catalytic activity for HER and the presence of additional C species in Co–Mo–C deposits could affect its catalytic activity through changing the overvoltage value of hydrogen evolution. Unfortunately, both microcracks and holes could be found on the two prepared alloy surfaces. However, the Co–Mo alloy co-deposition from these aqueous solution baths is always accompanied by intensive HER resulting in profound effect on quality of these Co–Mo alloys materials and current efficiency [26–28]. In addition, a few organic additives including crystallization control agents and complexing agents are generally employed to improve their electro-crystallization reaction and added into the bath during the Co–Mo co-deposition process, thus, these organic additives can also participate in the co-deposition process and the participation can also exhibit a profound effect on the quality and phase structure of these Co–Mo alloys materials [32, 33]. Another main issue associated with the Co–Mo alloys electrodeposition from aqueous solution baths is that a few microcracks [8, 12, 29, 30] and/or pinholes [28] could be found on the Co–Mo alloy materials surface. Normally, the two flaws can usually decrease their catalytic stability for HER. It should be noted that some effective techniques including pulse plating [34] or pulse-reverse plating [35] have been successfully developed to decrease these microcracks.

In recent years, the electrodeposition of Co and Co alloys (including Co–Mo alloys) from nonaqueous systems such as ionic liquid (IL) system, organic solvent, and the mixture of IL and organic solvent, has received intensive interest as reported in several literatures [24, 36–41] due to the fact that these techniques could eliminate the necessity to employ additional complexing agents, improve current efficiency, and obtain more variety of materials with better property compared with traditional aqueous systems. For instance, the Co and Co–Al alloys coatings without microcracks had been successfully prepared by Carlin et al. [41] from the 1.5:1.0 AlCl₃:1-ethyl-3-methylimidazolium chloride room temperature molten salt. The cobalt nanowires with an average diameter 45 nm were successfully electrodeposited by Yang et al. [40] from a mixture of 1-ethyl-3-methylimidazolium chloride IL and EG system, they found that these cobalt nanowires obtained from the mixture system showed a smoother surface and better magnetic properties than cobalt nanowires electrodeposited from aqueous solution. It should be noted that the IL system is extraordinary hygroscopicity, indicating that the

mixture IL system is not a better candidate for practical application in Co and Co alloys preparation. In addition, Costovici et al. [38] reported that Co–Mo alloy films with a nanocrystalline structure could be obtained from choline chloride based ILs and its surface morphology could be affected by technological conditions. It should be noted that many microcracks could also be observed on the obtained Co–Mo alloy coating surface. Although a few of literatures about Co and Co alloy films electrodeposited from organic solvents including such DMF [42], DMSO [43], and EG [37] have been published, the literatures about the Co–Mo alloy coatings prepared from organic solvents have been published hardly in previous literatures.

In our previous works, nanocrystalline Co coating with spherical crystal particles forming many wirelike crystals bundles was prepared from EG system [37]. Subsequently, both the nanocrystalline Co [36] and Co–Ni alloy [24] catalysts were electrodeposited from the [EMIM]HSO₄-EG system, and they exhibited a better catalytic activity and stability for HER. However, [EMIM]HSO₄ IL is relatively expensive due to its complex synthesis process and low productivity, thus, [EMIM]HSO₄-EG mixture as a plating system can significantly raise the production cost due to the extra IL. More importantly, nowadays, the Co–Mo alloys obtained from pure EG system and used as catalysts for HER have not been reported. Thus, EG solvent is employed as electrolyte to prepare Co–Mo deposits in this work, expecting that the obtained Co–Mo alloys can exhibit a prominent catalytic activity for HER. The co-deposition behavior of Co(II) and Mo(VI) and Co–Mo electro-crystallization mechanism in EG system are investigated by cyclic voltammetry (CV) and chronoamperometry (CA) measurements, respectively. The surface morphology, composition, and microstructure of the Co–Mo alloy films are observed using SEM, EDS, and XRD. Moreover, the catalytic performances of the obtained Co–Mo alloys catalysts are also investigated using linear sweep voltammetry (LSV), electrochemical impedance spectra (EIS), and CA techniques in 1 M KOH solution.

2 Experimental

2.1 Chemicals

EG ($\geq 99.5\%$), anhydrous CoCl₂ (99.7%), and Na₂MoO₄ ($\geq 99.5\%$) were obtained from Aladdin Bio-Chem Technology Co., Ltd (Shanghai). Before using, all the above three reagents were dried based on the previous literatures [36, 37]. All other chemicals and reagents used in this study were commercially available and of an analytical reagent grade.

2.2 Electrochemical measurements

The CV curves of the EG system containing various concentration of Co(II) and/or Mo (VI) were obtained at 323 K by a frequently used three-electrode construction with the help of a electrochemical workstation (CH Instruments CHI660B). It should be noted that the working electrode (WE) was GC electrode (exposed area: 0.07 cm²), the counter electrode was a graphite rod, and the reference electrode was saturated calomel electrode (SCE) using a ground glass joint type junction. Before using, the GC electrode was pretreated according to the previous literatures [36, 37]. It should be noted that the EG system was not stirred and the *IR* compensation was performed for these electrochemical measurements and plating experiments.

2.3 Preparation and characterization of Co–Mo deposits

Co–Mo alloy coatings with different Mo contents were electrodeposited using galvanostatic technique with the help of a DC power supply from the EG system containing 0.5 M Co(II) and different Mo(VI) concentrations (0.015–0.075 M) at 343 K. For plating experiments, the 99.9 wt% copper sheet (exposed area: 0.5 × 1.0 = 0.5 cm²) was used as the depositing substrate (cathode) and a platinum sheet (3 cm²) as the anode. The distance between the cathode and anode in the plating bath maintain 2 cm. It should be noted that the copper sheet (plating substrate) was also pretreated before

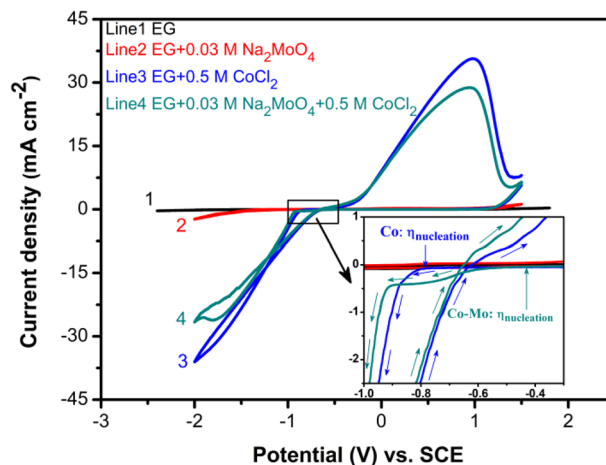


Fig. 1 Cyclic voltammograms of EG system (curve 1), EG system containing 0.5 M Co(II) (curve 2), EG system containing 0.03 M Mo(VI) (curve 3), and EG system containing 0.5 M Co(II) + 0.03 M Mo(VI) (curve 4) recorded on a GC electrode at 323 K with scan rate of 50 mV s⁻¹

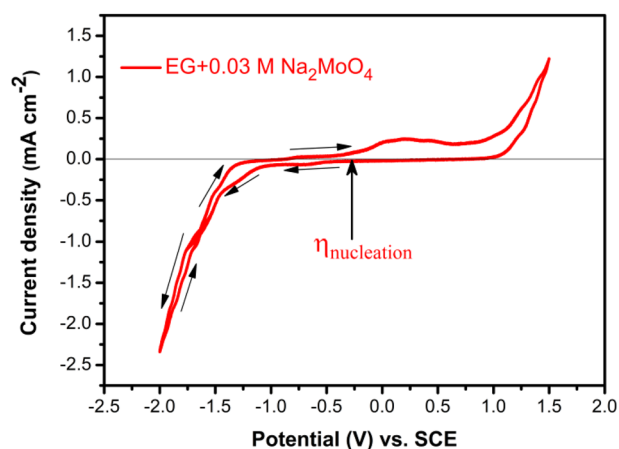


Fig. 2 Cyclic voltammogram of EG system containing 0.03 M Mo(VI) recorded on a GC electrode at 323 K with scan rate of 50 mV s^{-1}

plating and the copper sheet coated by Co–Mo deposits was treated after plating based on the previous literatures [31, 44]. It should be noted that preparation of Co–Mo deposits and all electrochemical measurements were performed in a glove box with an Ar atmosphere containing less than 2 ppm of oxygen and moisture.

Scanning electron microscope (TESCAN MIRA4) with an energy dispersive spectrometer (EDS) was used to observe the surface topography and the element analysis of the Co–Mo deposits, and their phase structures were observed by XRD using a Bruker D8 with Cu $K\alpha$ radiation.

2.4 Electrocatalytic measurements

The HER catalytic performances for the Co–Mo deposits were measured in 1 M KOH solution using LSV (scan rate: 1 mV s^{-1}), EIS, CV, and CA techniques at 298 K, respectively. It should be noted that the above-mentioned electrochemical workstation and three-electrode construction were also employed during LSV, EIS, CV, and CA measurements, the main variations were that the copper sheet coated by Co–Mo deposits (0.5 cm^2) was employed as working electrode and graphite rod as counter electrode. EIS curves were measured under 0.1 V vs. RHE overpotential (amplitude: 5 mV, frequency: 10^5 to 10^{-2} Hz). CV method with 1000 and 2000 cycles at scanning rate of 50 mV s^{-1} , as well as CA method, was carried out to confirm the catalytic stability of the Co–Mo deposits. It should be noted that the potentials in this study were converted into a reversible hydrogen electrode (RHE) potential according to the method reported in these literatures [19, 36].

3 Results and discussion

3.1 Cyclic voltammetry study

Figure 1 exhibits these representative CV curves of EG system containing 0.03 M Mo(VI) or/and 0.5 M Co(II) measured using a scan rate (ν) of 50 mV s^{-1} at 323 K. As shown in Fig. 1, EG system exhibits excellent electrochemical stability because no apparent reduction and oxidation peaks are recorded for the pure EG solution in the range from +1.500 to -2.000 V (curve 1), while all the other curves in Fig. 1 are obviously changed at the existence of 0.5 M Co or/and 0.03 M Mo(VI) in EG solvent. For curve 2, the cathodic current density increases clearly from -0.475 V (the so-called nucleation overpotential, $\eta_{\text{nucleation}}$) to -1.124 V (Fig. 2), and then a well-defined cathodic shoulder can be found between -1.124 and -1.781 V . During the reversal scanning, an obvious current density loop (crossover), indicating the existence of a nucleation and crystal growth process, can be found at -1.638 V , and the anodic current density peak is observed at 0.247 V , which is due to the anodic stripping of the electrodeposited Mo and/or molybdenum oxide onto the cathode surface. It should be noted that the electrochemical behavior for Mo(VI) in some ILs [38] or aqueous systems [45], there is not existence of such crossover of the cathodic and anodic branches due to the presence of molybdenum oxide (MoO_2) which dominates the active sites of nucleation and can impede Mo(VI) reduction to Mo. Thus, the result indicates that the nucleation and growth process for Mo in EG system is much easier than that of some ILs [38] or aqueous systems [45].

For curve 3 and 4, both the cathodic current densities improve sharply from -0.866 to -0.591 V to -1.625

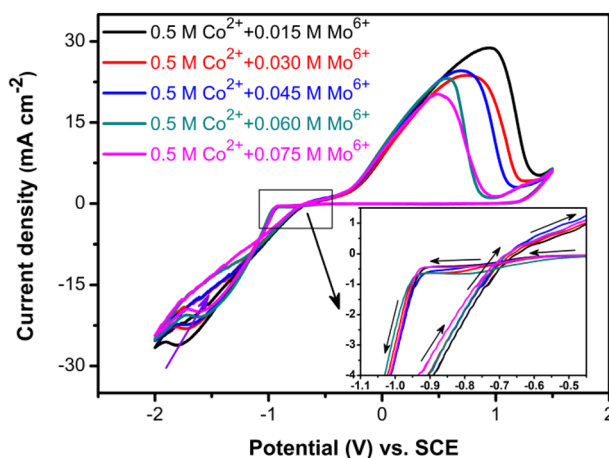


Fig. 3 Cyclic voltammograms of various Mo(VI) concentrations in EG system containing 0.5 M Co(II) recorded on a GC electrode at 323 K with scan rate of 50 mV s^{-1}

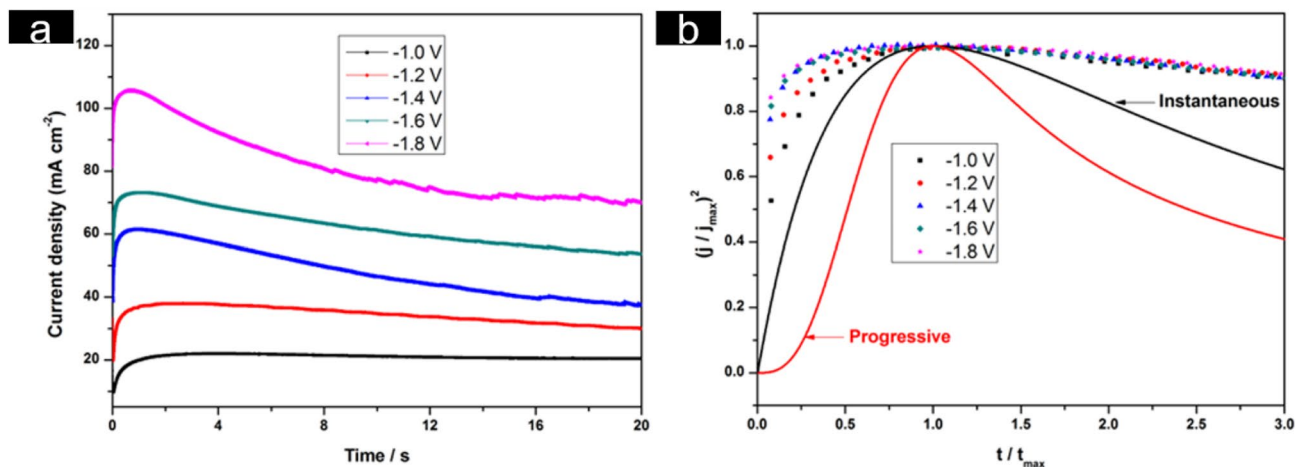


Fig. 4 Chronoamperometric current transient at different potentials in EG system containing 0.5 M Co(II) and 0.03 M Mo(VI) at 323 K (a). Comparison of dimensionless time-current curves with 3D nucleation model (b)

and -0.961 V, respectively, and a clear cathodic current density peak for curve 3 and a mild shoulder for curve 4 are observed. During the reversal scanning, two clear current density loops are observed at -1.225 (curve 3) and -1.144 V (curve 4), and the two corresponding anodic current density peaks are observed at 0.984 (curve 3) and 0.701 V (curve 4). The cathodic current density peak and cathodic shoulder are attributed to the Co(II) reduction to Co and the Co–Mo co-deposition, respectively, while two anodic density peaks can be attributed to the corresponding stripping of Co and Co–Mo alloy. Interestingly, the nucleation overpotential of Co–Mo co-deposition (-0.433 V) in EG is more positive than that of pure Mo, implying that the presence of extra Co(II) species in EG can facilitate Mo deposition process and there is a typical induced co-deposition. More interestingly, the cathode current density for curve 4 [0.5 M Co(II) and 0.03 M Mo(VI)] is smaller than that of curve 3 [only 0.5 M Co(II)] at the same potential during the cathodic scanning. These results indicate that the presence of additional Mo(VI) species in EG can inhibit the Co(II) reduction, and then their effect should be enhanced as Mo(VI) species concentration increases. In order to confirm the case, another CV measurement using scan rate (v) of 50 mV s^{-1} on GC at 323 K were performed in EG + 0.5 M Co(II) solution with the change of Mo(VI) concentration from 0.015 to 0.075 M and represents in Fig. 3. It can be found that the nucleation overpotential for the Co–Mo co-deposition is almost unchangeable, while the current density for cathodic peak (j_{cp}) decreases with the increase of Mo(VI) concentration. Thus, the result verifies the presence of Mo(VI) species in EG can obviously inhibit the co-deposition process. It should be noted that there are mild electrochemical noises in negative potential side for these CV curves in Fig. 3, it may be attributed to the change of local

active species and the adsorption of hydroxides and oxides of molybdenum on cathode surface.

3.2 Chronoamperometry study

Figure 4 represents these typical current-time transient curves for EG solution containing 0.5 M Co(II) and 0.03 M Mo(VI).

As shown in Fig. 4a, these transients present a representative shape for a diffusion-limited nucleation process with three-dimensional growth of a new phase [46, 47]. For their initial stage, because of the existence of many active sites on the non-ideal surface of the electrode, Co–Mo bimetallic clusters can radially grow using the active sites as the growth centers. It is worth noting that all these Co–Mo clusters are normally small with a steady-state and grow under the diffusion control. During the grow reaction process, the current density increasingly increases to a peak value due to the fact that there is no overlap among these diffusion layers. Whereafter, these diffusion regions around Co–Mo nuclei overlap and finally the growth for the Co–Mo alloy coatings is controlled by planar diffusion to the whole cathode electrode surface, and then the rate of nuclear growth is slow-down. Thus, all these current densities at the various applied potentials are decreased and gradually tend to level off. In order to further set forth the mechanism of Co–Mo alloy nucleation and growth process, non-dimensional $(j/j_{max})^2$ vs. (t/t_{max}) curves proposed by Sharifker–Hills [48] were employed based on Eqs. 1 and 2 from current-time transient curves and shown in Fig. 4b.

$$\frac{j^2}{j_{max}^2} = \frac{1.9542}{t/t_{max}} \left[1 - \exp\left(-1.2564 \frac{t}{t_{max}}\right) \right]^2 \quad (1)$$

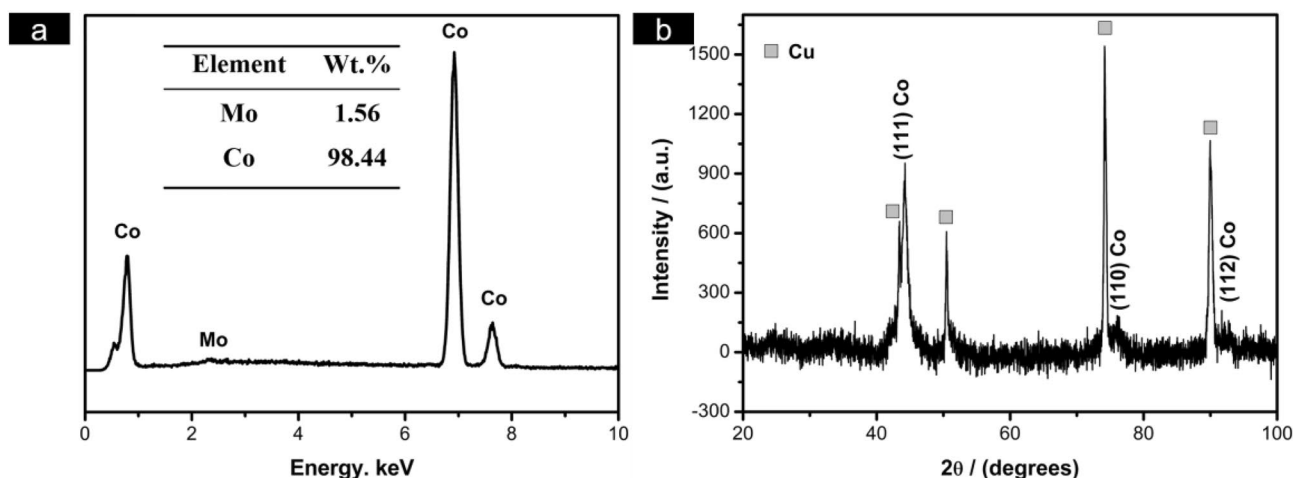


Fig. 5 EDS analysis (a) XRD pattern (b) of these deposits prepared at 20 mA cm^{-2} for 30 min from EG system containing 0.5 M Co(II) and 0.03 M Mo(VI) at 343 K

(Instantaneous nucleation)

$$\frac{j^2}{j_{\max}^2} = \frac{1.2254}{t/t_{\max}} \left[1 - \exp\left(-2.3367 \frac{t^2}{t_{\max}^2}\right) \right]^2 \quad (2)$$

(Progressive nucleation)

where j is the current density, t is the time, and j_{\max} is the maximum current density at time t_{\max} . As shown in Fig. 4b, it can draw a conclusion that the Co–Mo alloy nucleation is principally an instantaneous nucleation regime at the various applied potentials at 323 K.

3.3 Characterization of Co–Mo alloy deposits

Figure 5a represents a representative EDS analysis of the Co–Mo alloy deposits prepared 20 mA cm^{-2} for 30 min from EG system containing 0.5 M Co(II) and 0.03 M Mo(VI) at 343 K. As shown in Fig. 5a, these deposits principally consist of Co (98.44 wt%) and Mo (1.56 wt%). The result indicates that these deposits are the cobalt enriched Co–Mo alloy. Figure 5b represents a representative XRD pattern of the Co–Mo alloy deposits obtained 20 mA cm^{-2} for 30 min from EG system containing 0.5 M Co(II) and 0.03 M Mo(VI) at 343 K. As shown in Fig. 5b, four intense copper peaks are found in the spectra, indicating that the thickness for the obtained Co–Mo deposits is so thin that the substrate copper is observed. Meanwhile, an intense peak and two mild peaks correspond to (111), (110), and (112) peaks of phase Co according to PDF#97-004-4989. However, the diffraction peaks associated to the metallic Mo are not observed, implying that the fact that the Mo atoms form a phase Co (Mo) solid solution through entering the Co crystal lattices [8].

Figure 6 represents the representative surface morphology of these Co–Mo deposits with different Mo contents. As shown in Fig. 6, the surface morphology of the prepared Co–Mo deposits is obviously influenced by Mo content, and their microstructure can change from a fibrous structure (Fig. 6a and b) to spherical structure (Fig. 6c, d and e) as Mo content increases. Moreover, when the Mo content is relatively low, the fibrous microstructure also changes from fur structure with many bundles of elongated crystals randomly distributed throughout the deposits surface (Fig. 6a) to pure pompon microstructure (Fig. 6b) (more clearly defined at a higher resolution in Fig. 6f), and the average size of these fibrous structures is decreased as the increase of Mo content from 0.07 to 1.56 wt%. Normally, pompon structure with innumerable fine fur (Fig. 6b) owns a larger electrochemical active surface area (ECSA) than that of “simple” spherical structure (Fig. 6c, d and e) and then it can exhibit a better electrocatalytic performance of hydrogen evolution. Thus, the Co–Mo deposits with 1.56 wt% Mo should present a better electrocatalytic property. In addition, as shown in Fig. 6g, the thickness of the obtained deposits is about $7.257 \mu\text{m}$.

Moreover, X-ray photoelectron spectroscopy (XPS) analysis is employed to confirm the chemical valence states and elemental composition of Co–Mo alloy and shown in Fig. 7. The spectral peaks in survey spectrum verify the presence of Co and Mo elements (Fig. 7a). For the Co 2p region of Co–Mo alloy (Fig. 7b), the spectrum can be divided into four peaks, located at Co $2p_{3/2}$ with four binding energies (BEs) (778.56, 780.77, 782.27, and 786.35 eV), which correspond Co^0 , Co^{2+} , Co^{3+} species and a shake-up satellite peak, respectively [49]. For the Co $2p_{1/2}$ profile, it can be divided into three peaks,

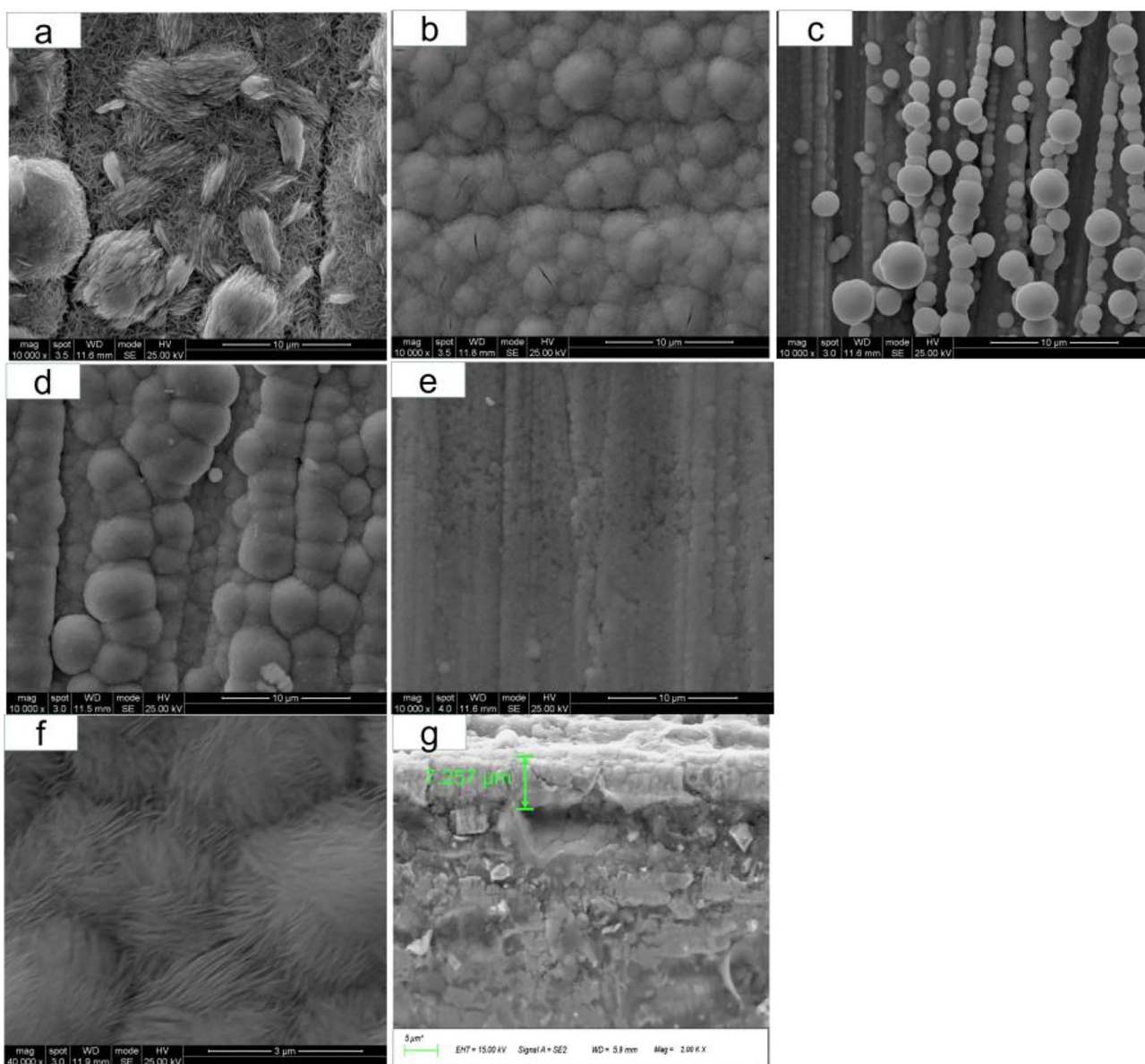


Fig. 6 SEM micrographs of Co–Mo deposits with different Mo contents prepared at 20 mA cm^{-2} for 30 min from EG system at 343 K. **a** 0.07 wt%, **b** 1.56 wt%, **c** 4.46 wt%, **d** 5.30 wt%, **e** 19.90 wt%, **f** the

enlargement of micrograph (**b**); **g** cross sectional SEM image of Co–Mo deposits with the Mo content of 1.56 wt%

corresponding Co^{2+} , Co^{3+} and shake-up satellite peaks, with three BEs (796.04, 797.83, and 802.88 eV), respectively. For the Mo 3d region of Co–Mo alloy (Fig. 7c), the spectrum can be divided into two peaks, situated at Mo $3d_{5/2}$ with two BEs (231.45 and 232.75 eV) and Mo $3d_{3/2}$ with two BEs (235.07 and 235.92 eV), which Mo^{4+} species corresponding to hydroxide and oxidized forms [50, 51], respectively. It should be noted that the weight ratio of Co to Mo calculated by the XPS measurement is 98:2 (Co:Mo), which is similar to the result from EDS.

3.4 Electrocatalytic properties of Co–Mo deposits for HER

Figure 8a represents these representative LSV curves of the prepared Co–Mo deposits with different Mo contents. As shown in Fig. 8a, all these Co–Mo deposits prepared from EG system exhibit remarkable electrocatalytic activity for HER and the catalytic activity is clearly influenced by Mo content. The value of HER overpotential for catalytic current density reaching 10 mA cm^{-2} (η_{10}) diminishes as Mo content increases from 0.07 to 1.56 wt%. On the contrary, its value is obviously increased when the Mo content is over

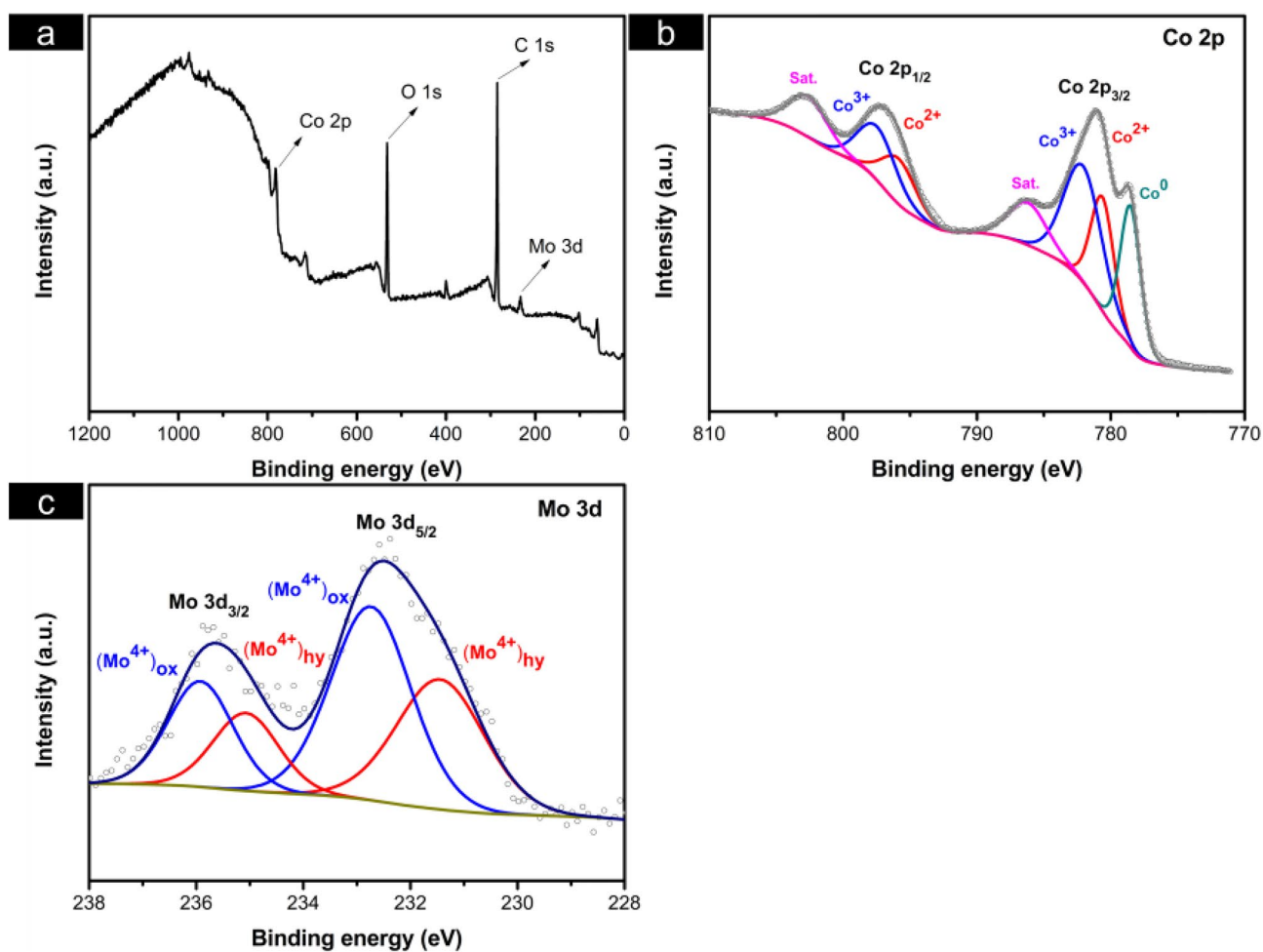


Fig. 7 XPS spectra of Co–Mo alloy with the Mo content of 1.56 wt%: XPS survey spectrum (a), Co 2p (b) and Mo 3d (c)

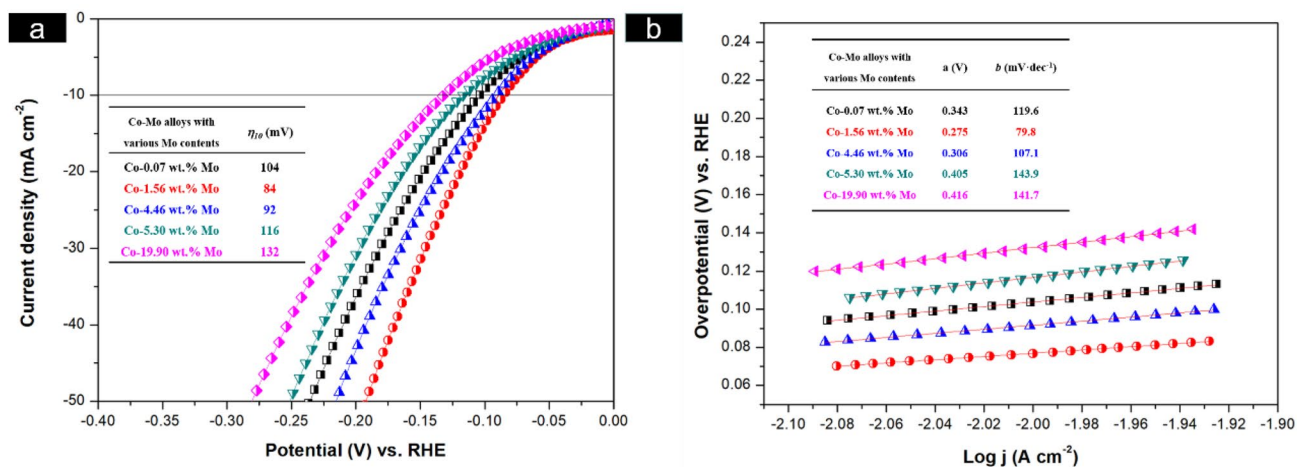


Fig. 8 Polarization curves (a) and Tafel plots b of Co–Mo deposits prepared from EG system in 1 M KOH solution at 298 K

Table 1 Comparison of HER activity, surface morphology and Mo content of obtained Co–Mo alloy electrocatalysts with previously reported Co–Mo alloys

Co–Mo alloys	Employed electrolytes	Mo content	Surface morphology	η_{10} ^a (mV)	b (mV·dec ⁻¹)	References
Co–Mo	Aqueous solution	27.40 at%	Spherical nodules structure with some cracks	– 156	83	[12]
Co–Mo	Aqueous solution	34.90 wt%	Spherical nodules structure with some microcracks	– 109	72	[53]
NiCoMo	Aqueous solution	5.00 at%	Dense 3D dendritic structure	– 132	108	[54]
CoMoCu	Aqueous solution	18.60 at%	Cauliflower-like structure	– 119	82	[12]
Co–Mo	EG	1.56 wt%	Pompon structure	84	79.8	This work

^aOverpotential (η_{10}) was recorded at $j = 10 \text{ mA cm}^{-2}$

1.56 wt%. The outstanding electrocatalytic activity for HER is also due to the modification of the crystalline structure when Mo atom is added into the structure of the iron group Co element, and then a remarkable synergistic effect can happen by means of the alloying of hyper d-electronic phase Co, which is the primary source of catalytic activity, and hypo d-electronic phase Mo, which is favorable for hydrogen adsorption [52]. That is to say, the enormous electrocatalytic activity can put down to the cooperative action of the Co and Mo dual atoms sites. For H_2 evolution of water electrolysis, Co atoms in these Co–Mo deposits act as the reaction sites employed by O–H bond cleavage of H_2O and then Mo atoms can act as the H_2 -evolving centers.

In addition, the bonding energy between Co–Mo alloy deposits with 1.56 wt% Mo and the hydrogen can meet the relative balance of the rate of adsorption and desorption reaction. Thus, the Co–Mo deposits with 1.56 wt% Mo present the expected and best HER catalytic activity with an overpotential of 84 mV (η_{10}). The result is in accordance with SEM observations. Farther, the HER overpotential value (84 mV) for the Co–Mo alloy deposits with 1.56

wt% Mo obtained from the EG system is smaller than that of other mainly electrodeposited nanostructured Co–Mo alloys [12, 53] and some ternary Co–Mo alloys catalysts [12, 54] for HER (Table 1). Compared with these Co–Mo alloy catalysts obtained from aqueous solutions (Table 1), the better catalytic activity of the Co–Mo deposits with 1.56 wt% Mo can mainly be correlated with its surface morphology and microstructure. It can be observed that the deposits present a new fibrous surface morphology with a pompon microstructure. Thus, the surface with the pompon structure should exhibit relatively larger specific surface area and then more active sites can be exposed to satisfy the HER compared with other morphologies including spherical nodular structure [12], dendritic structure [54], and cauliflower-like structure [13].

Normally, much valuable information on kinetics and the mechanism of HER can be acquired using Tafel technique [12, 54]. Thus, these Tafel curves are also extracted from LSV curves (Fig. 8a) and shown in Fig. 8b. In alkaline system, it is generally accepted that the HER consists of three electrochemical reaction steps, namely Volmer, Heyrovsky,

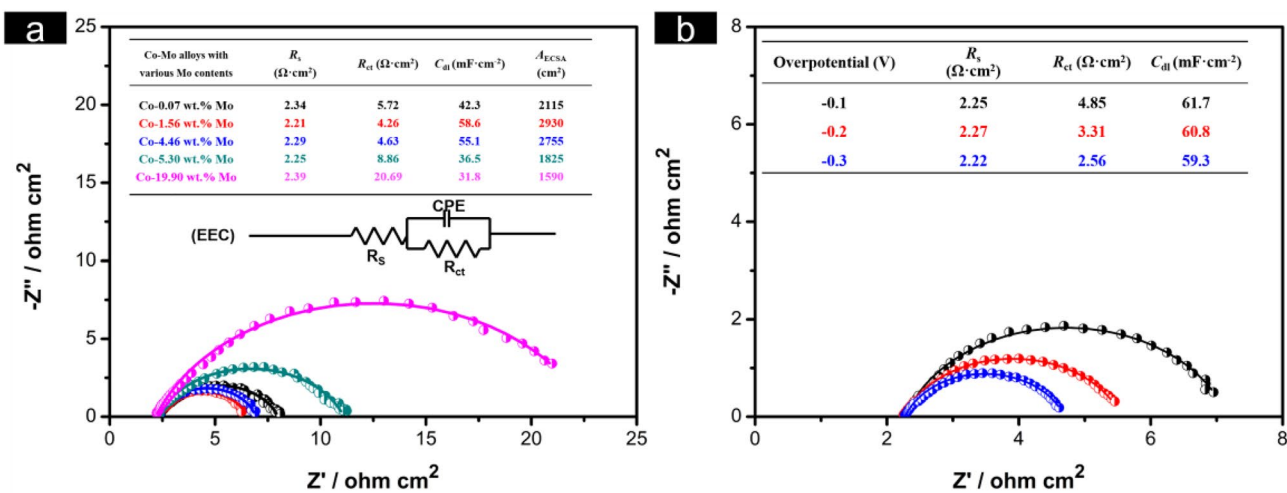
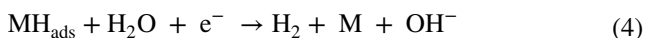
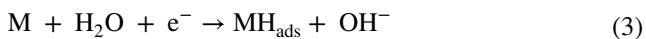


Fig. 9 Nyquist plots of Co–Mo deposits with different Mo content (a) and Co–Mo alloy catalyst with 1.56 wt% Mo in different overpotential b prepared from EG system in 1 M KOH solution at 298 K

and Tafel reactions. The first step is the electro-sorption proton discharge on catalyst [Volmer reaction; Eq. (3)], and then it is followed by an electro-desorption step [Heyrovsky's reaction; Eq. (4)] or the chemical-desorption step [Tafel reaction; Eq. (5)] to form hydrogen [54]:



In addition, the Tafel slope is extensively used to confirm the HER mechanism: Volmer–Heyrovsky or Volmer–Tafel model. Based on the Volmer–Heyrovsky mechanism, if the Volmer reaction is the rate-determining step of the overall reaction, then the Tafel slope should be 120 mV dec^{-1} , and if the Heyrovsky's and Tafel reactions are the rate-determining steps, then the Tafel slope should be 40 and 30 mV dec^{-1} , respectively. As shown in Fig. 8b, all the Tafel slopes are in the range of 79.8 to $143.9 \text{ mV dec}^{-1}$, indicating that the HER on Co–Mo deposits nearly belongs to a Volmer adsorption process as its rate-determining step. The Tafel slope (79.8 mV dec^{-1}) of the Co–Mo deposits with 1.56 wt% Mo is also lower than that of other Co–Mo alloys with different Mo contents obtained from the EG system, and also lower than that of other mainly electrodeposited nanostructured Co–Mo alloys (Table 1), implying that the Co–Mo alloy with 1.56 wt% Mo is more favorable for HER catalytic kinetics.

In addition, some valuable information on HER kinetics and the interface properties on an electrocatalyst surface can also be obtained using EIS technique [12]. Therefore, the EIS measurements for these Co–Mo alloy deposits with different Mo contents used as HER electrocatalysts have been

carried out in 1 M KOH system and shown in Fig. 9a. Additionally, the EIS data is fitted by Zview software according to the electrical equivalent circuit (EEC) (the inset in Fig. 9a) and the obtained data are also listed in Fig. 9a. Where R_s is solution resistance; CPE (constant phase element) is related to the double layer capacitance (C_{dl}); R_{ct} is the electrochemical charge transfer resistance. Moreover, the obtained EIS parameters that correspond to the HER charge transfer kinetics, can be used to calculate the ECSA [12], and then the obtained ECSA values for various Co–Mo alloys are also shown in Fig. 9a. As exhibited in Fig. 9a, both the conductivity and HER catalytic activity of these Co–Mo alloy deposits can be obviously influenced by Mo content. The semicircle diameter minishes as Mo content increases from 0.07 to 1.56 wt%. The result indicates that the conductivity and HER catalytic activity are increased. Inversely, the semicircle diameter increases as the Mo content is over 1.56 wt%. The result indicates that their conductivity and HER catalytic activity are minished. Moreover, the Co–Mo deposits catalyst with 1.56 wt% Mo presents the smallest HER internal resistance and charge transfer resistance, which means that the electron transfer speed is faster on the surface of the Co–Mo alloy catalyst, thereby exhibiting more better catalytic performance for HER. In addition, these data information on ECSA presents that Co–Mo deposits catalyst with 1.56 wt% Mo presents a bigger value (2930 cm^2) in comparison to other Co–Mo deposits with various Mo contents, also implying a better electrocatalytic activity. In order to further investigate the kinetics of HER on the Co–Mo alloy catalyst with 1.56 wt% Mo, the EIS measurements of the Co–Mo alloy catalyst with 1.56 wt% Mo in different overpotential (-0.1 , -0.2 , and -0.3 V vs. RHE) have been carried out and shown in Fig. 9b. As shown in Fig. 9b, the radius of the semicircle is decreased with the increase of the

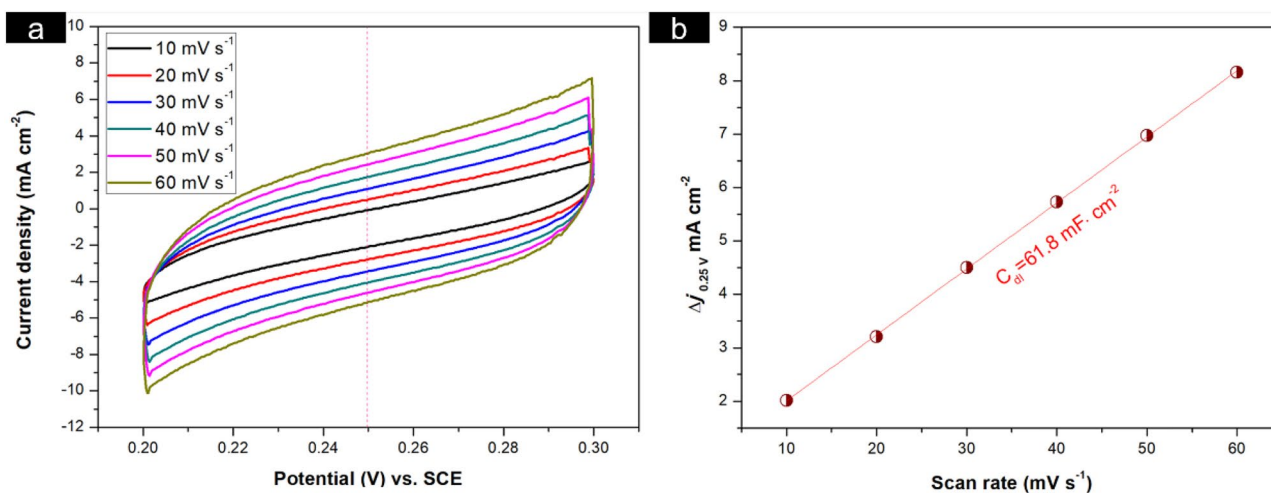


Fig. 10 CVs of Co–Mo deposits with 1.56 wt% Mo measured in a non-Faradaic region of the voltammogram at different rates from 10 to 50 mV s^{-1} in 1 M KOH (a). The capacitive current density at 0.25 V vs. RHE as a function of scan rate for the Co–Mo deposits (b)

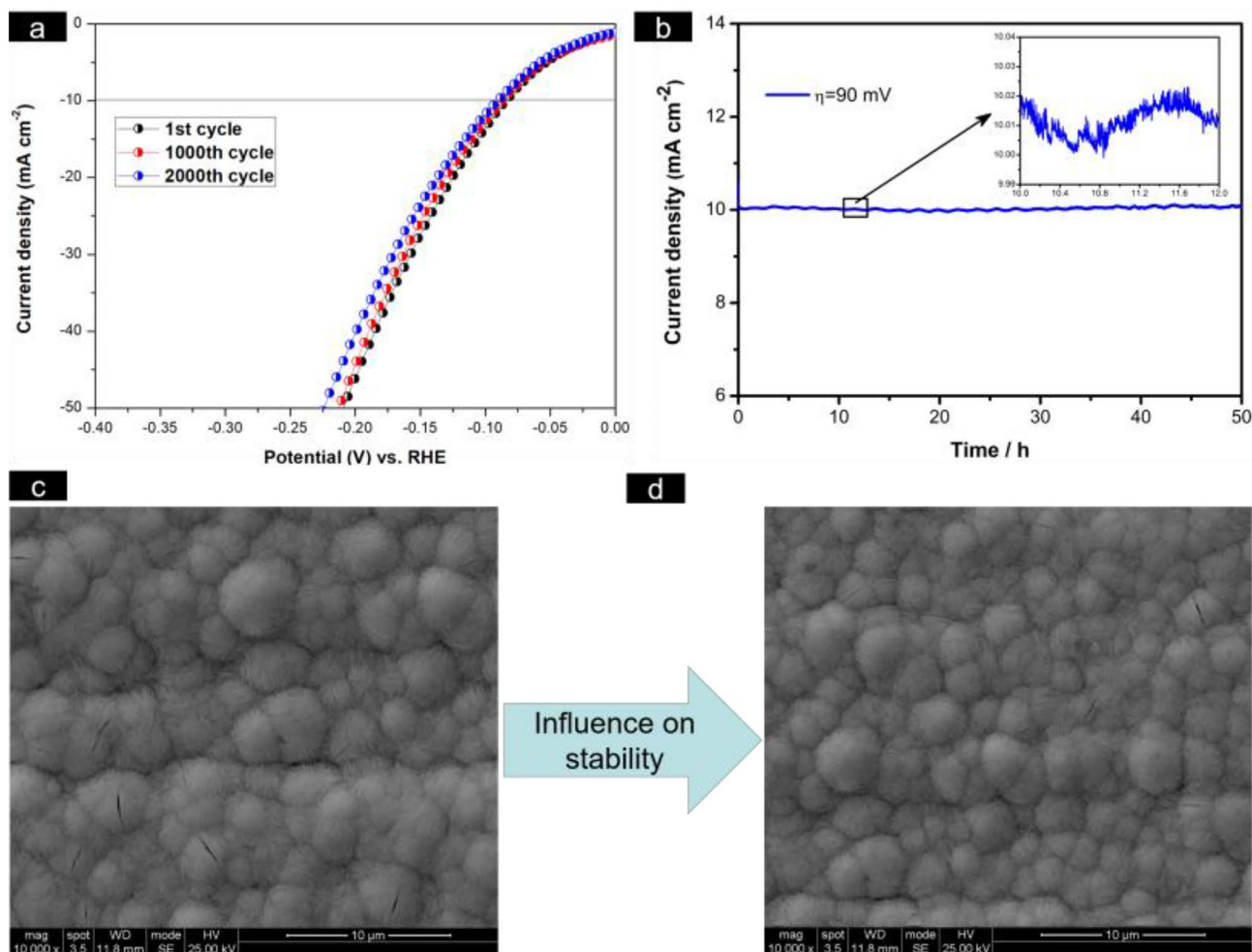


Fig. 11 Polarization curves for Co–Mo alloy deposits with 1.56 wt% Mo initial recorded and after 1000 and 2000 cycles (a); chronoamperometry curve for Co–Mo alloy deposits with 1.56 wt% Mo during

electrolysis about 10 h at overpotential 90 mV (b). SEM image before (c) and after d stability test

overpotential, implying an improvement in the HER kinetics with an increase of the overpotential. It should be noted that the C_{dl} value (inset in Fig. 9b) is nearly constant with the increase of the overpotential. Generally, the C_{dl} values should be reduced with the increase of overpotential due to the aggregation of hydrogen bubbles on the catalyst surface [55]. Based on the fact, it can be drawn a conclusion that the hydrogen bubbles cannot aggregate on the surface with the pompon structure and are instead rapidly separated from the surface once they are formed. These results are in keeping with the LSV measurements.

Normally, electrochemical active surface area (ECSA) is an essential parameter associated with the HER electrocatalytic activity [44, 56], and electrochemical capacitance (C_{dl}) can be used to estimate the ECSA value using the C_{dl} value for a flat standard with 1 cm^2 of real surface area [57]. Moreover, the C_{dl} value for a flat surface is normally considered to be in the range of $20\text{--}60 \mu\text{F cm}^{-2}$. In addition, the

electrochemical capacitance (C_{dl}) can be acquired by CV technique in a potential range where no faradic processes with various scan rates to calculate the ECSA value [44, 56, 57]. Therefore, the potential is recorded between 0.2 and 0.3 V vs. RHE at different rates from 10 to 60 mV s^{-1} in 1 M KOH. The typical CV curves for the Co–Mo deposits with 1.56 wt% Mo is recorded in Fig. 10a and the capacitive current density at 0.25 V vs. RHE as a function of scan rate for the Co–Mo deposits is recorded in Fig. 10b. The calculated C_{dl} for the Co–Mo deposits with 1.56 wt% Mo is about 61.8 mF cm^{-2} . Therefore, in this study, the ECSA value of the Co–Mo deposits is evaluated to be 3090 cm^2 using $20 \mu\text{F cm}^{-2}$ for a lower limit. The value (3090 cm^2) is bigger than that of the electrodeposited nanostructured Co–Mo alloys (1331 cm^2) [10], indicating that these Co–Mo deposits obtained from EG exhibit a better electrocatalytic property. More importantly, the value is in line with the EIS

measurements ($ECSA = 2930 \text{ cm}^2$), implying that this study is reliable.

Another main property of an HER catalysts is the catalytic stability. Thus, CV and chronoamperometry techniques are employed to assess the catalytic stability of Co–Mo deposits with 1.56 wt% Mo that exhibited the best HER electrocatalytic property. Figure 11a presents these typical polarization plots of Co–Mo deposits with 1.56 wt% Mo before and after performing 1000 or 2000 CV scans. It is obvious that these curves exhibit only a puny change in HER overpotential after 1000 cycles (4 mV) and after 2000 cycles (5 mV), which can be attributed to the high electrocatalytic stability of the Co–Mo deposits electrocatalysts. To confirm the stability, the chronoamperometry curve of the Co–Mo deposits electrocatalysts with 1.56 wt% Mo is measured in 1 M KOH by applying an overpotential $\eta = 90 \text{ mV}$ and exhibited in Fig. 11b. As shown in Fig. 11b, during the 50 h testing, it can be observed that the current density ($10.0 \pm 0.05 \text{ mA cm}^{-2}$) throughout the electrolysis period remains constant. Therefore, the electrocatalytic stability of the obtained Co–Mo alloy electrocatalysts from EG system presents an excellent stability for HER in alkaline system. Figure 11c and d show SEM images taken before and after the stability test respectively. It is evident that the surface morphology has not changed during the stability test due to the electrolysis of water, indicating that the Co–Mo deposits electrocatalysts with 1.56 wt% Mo has outstanding catalytic stability of HER.

4 Conclusion

- (1) Co–Mo co-deposition in EG system is a representative induced deposition.
- (2) The extra Co(II) species in EG can facilitate Co–Mo co-deposition, inversely, Mo(VI) species can inhibit Co(II) reduction and the effect can be enhanced as Mo(VI) concentration increases.
- (3) Co–Mo deposits with a pure pompon microstructure can be prepared from EG system and the EG system is a promising candidate for commercial application in Co–Mo alloys plating.
- (4) Benefiting from the composition engineering by alloying with Mo, as well as the simultaneous presence of a suitable pompon structure, the Co–Mo deposits with 1.56 wt% Mo exhibit a high HER electrocatalytic activity and stability with an overpotential of 84 mV at 10 mA cm^{-2} in 1 M KOH solution. Thus, the prepared Co–Mo catalysts are promising candidates for practical hydrogen production in alkaline solution.

Acknowledgements The authors acknowledge the financial supports of the National Natural Science Foundation of China (No. 21476067) and the Project Sponsored by the Scientific Research Foundation for the Returned Overseas Chinese Scholars, State Education Ministry.

Author contributions XH: conceptualization, methodology, writing—original draft, review & editing. RG: investigation, data curation, writing—original draft. ZH: investigation, data curation, writing—original draft. QZ: investigation, data curation, writing—original draft. JY: data curation, visualization. LW: writing—original draft, funding acquisition, validation.

Declarations

Competing interests The authors declare that they have no known competing financial interests or personal relationships that could have appeared to influence the work reported in this paper.

References

1. Panwar NL, Kaushik SC, Kothari S (2011) Role of renewable energy sources in environmental protection: a review. *Renew Sustainable Energy Rev* 15:1513–1524. <https://doi.org/10.1016/j.rser.2010.11.037>
2. Alaba PA, Abbas A, Daud WMW (2017) Insight into catalytic reduction of CO_2 : catalysis and reactor design. *J Clean Prod* 140:1298–1312. <https://doi.org/10.1016/j.jclepro.2016.10.022>
3. Spinner NS, Vega JA, Mustain WE (2012) Recent progress in the electrochemical conversion and utilization of CO_2 . *Catal Sci Technol* 2:19–28. <https://doi.org/10.1039/C1CY00314C>
4. Wang J (2015) Barriers of scaling-up fuel cells: cost, durability and reliability. *Energy* 80:509–521. <https://doi.org/10.1016/j.energy.2014.12.007>
5. Gupta NM (2017) Factors affecting the efficiency of a water splitting photocatalyst: a perspective. *Renew Sustainable Energy Rev* 71:585–601. <https://doi.org/10.1016/j.rser.2016.12.086>
6. Santos HLS, Corradini PG, Andrade MAS, Mascaro LH (2020) CuO/NiOx thin film–based photocathodes for photoelectrochemical water splitting. *J Solid State Electrochem* 24:1899–1908. <https://doi.org/10.1007/s10008-020-04513-5>
7. Zabinski PR, Nemoto H, Meguro S, Asami K, Hashimoto K (2003) Electrodeposited Co–Mo–C cathodes for hydrogen evolution in a hot concentrated NaOH solution. *J Electrochem Soc* 150(10):C717–C722. <https://doi.org/10.1149/1.1604788>
8. Casciano PNS, Benevides RL, Santana RAC, Correia AN, de Lima-Neto P (2017) Factorial design in the electrodeposition of co-mo coatings and their evaluations for hydrogen evolution reaction. *J Alloys Compd* 723:164–171. <https://doi.org/10.1016/j.jallcom.2017.06.282>
9. Wang C, Podlaha EJ (2020) Communication-electrodeposited Co–Mo–P–TiO₂ composites electrocatalysts for the hydrogen evolution reaction. *J Electrochem Soc* 167:132502. <https://doi.org/10.1149/1945-7111/abb7e7>
10. Laszczyńska A, Szczygieł I (2020) Electrocatalytic activity for the hydrogen evolution of the electrodeposited Co–Ni–Mo, Co–Ni and Co–Mo alloy coatings. *Int J Hydrogen Energy* 45:508–520. <https://doi.org/10.1016/j.ijhydene.2019.10.181>
11. Kuznetsov VV, Gamburg YD, Zhalnerov MV, Zhulikov VV, Batalov RS (2016) Reaction of hydrogen evolution on Co–Mo (W) and Ni–Re electrolytic alloys in alkaline media. *Russ J Electrochem* 52:901–909. <https://doi.org/10.1134/S1023193516090068>

12. Santos HLS, Corradini PG, Medina M, Mascaro LH (2020) Effect of copper addition on cobalt-molybdenum electrodeposited coatings for the hydrogen evolution reaction in alkaline medium. *Int J Hydrogen Energy* 45:33586–33597. <https://doi.org/10.1016/j.ijhydene.09.128>
13. Kuznetsov VV, Kalinkina AA, Pshenichkina TV, Balabaev VV (2009) Electrocatalytic properties of cobalt-molybdenum alloy deposits in the hydrogen evolution reaction. *Russ J Electrochem* 44:1350–1358. <https://doi.org/10.1134/S1023193508120070>
14. Kuznetsov VV, Gamburg Y, Zhulikov VV, Krutskikh VM, Filatova EA, Trigub AL et al (2020) Electrodeposited NiMo, CoMo, ReNi, and electroless NiReP alloys as cathode materials for hydrogen evolution reaction. *Electrochim Acta* 354:136610. <https://doi.org/10.1016/j.electacta.2020.136610>
15. Khajehsaeidi Z, Sangpour P, Ghaffarinejad A (2019) A novel co-electrodeposited Co/MoSe₂/reduced graphene oxide nanocomposite as electrocatalyst for hydrogen evolution. *Int J Hydrogen Energy* 44:19816–19826. <https://doi.org/10.1016/j.ijhydene.2019.05.161>
16. Jiao FX, Wang JL, Lin Y, Li JH, Jing XF, Gong YQ (2021) Sliver nanoparticles decorated co-mo nitride for efficient water splitting. *Appl Surf Sci* 553:149440. <https://doi.org/10.1016/j.apsusc.2021.149440>
17. Zhou XF, Yang XL, Hedhili MN, Li HN, Min SX, Ming J et al (2017) Symmetrical synergy of hybrid Co₉S₈-MoS_x electrocatalysts for hydrogen evolution reaction. *Nano Energy* 32:470–478. <https://doi.org/10.1016/j.nanoen.2017.01.011>
18. Roger I, Moca R, Miras HN, Crawford KG, Moran DAJ, Ganin AY et al (2017) The direct hydrothermal deposition of cobalt-doped MoS₂ onto fluorine-doped SnO₂ substrates for catalysis of the electrochemical hydrogen evolution reaction. *J Mater Chem A* 5:1472–1480. <https://doi.org/10.1039/C6TA08287D>
19. Wang C, Bilan HK, Podlaha EJ (2019) Electrodeposited Co-Mo-TiO₂ Electrocatalysts for the hydrogen evolution reaction. *J Electrochem Soc* 166:F661–F669. <https://doi.org/10.1149/2.1091910jes>
20. Patel PP, Hanumantha PJ, Datta MK, Velikokhatnyi OI, Hong D, Poston JA et al (2017) Cobalt based nanostructured alloys: versatile high performance robust hydrogen evolution reaction electro-catalysts for electrolytic and photo-electrochemical water splitting. *Int J Hydrogen Energy* 42:17049–17062. <https://doi.org/10.1016/j.ijhydene.2017.05.175>
21. Zhang WX, Cui L, Liu JQ (2020) Recent advances in cobalt-based electrocatalysts for hydrogen and oxygen evolution reactions. *J Alloys Compd* 821:153542. <https://doi.org/10.1016/j.jallcom.2019.153542>
22. Guo Y, Park T, Yi JW, Henzie J, Kim J, Wang Z et al (2019) Nano-architectonics for transition-metal-sulfide-based electrocatalysts for Water Splitting. *Adv Mater* 31:e1807134. <https://doi.org/10.1002/adma.201807134>
23. Ding H, Xu GC, Zhang L, Wei B, Hei JC, Chen L (2020) A highly effective bifunctional catalyst of cobalt selenide nanoparticles embedded nitrogen-doped bamboo-like carbon nanotubes toward hydrogen and oxygen evolution reactions based on metal-organic framework. *J Colloid Interface Sci* 566:296–303. <https://doi.org/10.1016/j.jcis.2020.01.096>
24. He XK, Sun ZY, Zou QT, Yang JJ, Wu LY (2019) Codeposition of nanocrystalline co-ni catalyst based on 1-ethyl-3-methylimidazolium bisulfate and ethylene glycol system for hydrogen evolution reaction. *J Electrochem Soc* 166:D908–D915. <https://doi.org/10.1149/2.0171916jes>
25. Han Q, Cui S, Pu NW, Chen JS, Liu KR, Wei XJ (2010) A study on pulse plating amorphous Ni–Mo alloy coating used as HER cathode in alkaline medium. *Int J Hydrogen Energy* 35:5194–5201. <https://doi.org/10.1016/j.ijhydene.2010.03.093>
26. Gómez E, Pellicer E, Vallés E (2004) Electrodeposition of soft-magnetic cobalt–molybdenum coatings containing low molybdenum percentages. *J Electroanal Chem* 568:29–36. <https://doi.org/10.1016/j.jelechem.2003.12.032>
27. Gómez E, Pellicer E, Vallés E (2004) Microstructures of soft-magnetic cobalt–molybdenum alloy obtained by electrodeposition on seed layer/silicon substrates. *Electrochem Commun* 6:853–859. <https://doi.org/10.1016/j.elecom.2004.06.011>
28. Gmez E, Pellicer E, Alcob X, Valls E (2004) Properties of Co-Mo coatings obtained by electrodeposition at pH6.6. *J Solid State Electrochem* 8:497–504. <https://doi.org/10.1007/s10008-004-0495-z>
29. Kublanovsky VS, Yapontseva YS (2014) Electrocatalytic properties of co-mo alloys electrodeposited from a citrate-pyrophosphate electrolyte. *Electrocatalysis* 5:372–378. <https://doi.org/10.1007/s12678-014-0197-y>
30. Žabiński P, Mech K, Kowalik R (2012) Co-mo and co-mo-c alloys deposited in a magnetic field of high intensity and their electrocatalytic properties. *Arch Metall Mater* 57:127–133. <https://doi.org/10.2478/v10172-012-0001-z>
31. Abdolmaleki M, Bodaghi A, Hosseini J, Jamehbozorgi S (2018) Preparation of nanostructured co-mo alloy electrodes and investigation of their electrocatalytic activity for hydrazine oxidation in alkaline medium. *J Chin Chem Soc* 65:970–976. <https://doi.org/10.1002/jccs.201700344>
32. Fekih Z, Ghellai N, Fortas G, Chiboub N, Sam S, Chabanne-sari NE et al (2011) Influence of the additives and the pH on the cobalt-molybdenum (Co-Mo) alloy electrodeposited on n-type silicon. *Phys Procedia* 21:101–107. <https://doi.org/10.1016/j.phpro.2011.10.015>
33. Gómez E, Pellicer E, Vallés E (2005) Developing plating baths for the production of cobalt–molybdenum films. *Surf Coat Technol* 197:238–246. <https://doi.org/10.1016/j.surfcoat.2004.09.017>
34. Pellicer E, Gómez E, Vallés E (2006) Use of the reverse pulse plating method to improve the properties of cobalt–molybdenum electrodeposits. *Surf Coat Technol* 201:2351–2357. <https://doi.org/10.1016/j.surfcoat.2006.04.011>
35. Cesiulis H, Tsyntaru N, Budreika A, Skridaila N (2011) Electrodeposition of CoMo and CoMoP alloys from the weakly acidic solutions. *Surf Eng Appl Electrochem* 46:406–415. <https://doi.org/10.3103/s1068375510050030>
36. He XK, Sun ZY, Zou QT, Wu LY, Jiang JB (2019) Electrochemical behavior of Co(II) reduction for preparing nanocrystalline Co catalyst for hydrogen evolution reaction from 1-ethyl-3-methylimidazolium bisulfate and ethylene glycol system. *J Electrochem Soc* 166:D57–D64. <https://doi.org/10.1149/2.0981902jes>
37. He XK, Yang JJ, Zou QT, Hu ZS, Wu LY (2022) Effects of deposition potential and temperature on Co(II) reduction and electrocrystallization for preparing nanocrystalline Co coatings in ethylene glycol solution. *J Electrochem Soc* 169:022502. <https://doi.org/10.1149/1945-7111/ac4e57>
38. Costovici S, Manea A-C, Visan T, Anicai L (2016) Investigation of Ni-Mo and Co-Mo alloys electrodeposition involving choline chloride based ionic liquids. *Electrochim Acta* 207:97–111. <https://doi.org/10.1016/j.electacta.2016.04.173>
39. Anicai L, Costovici S, Cojocar A, Manea A, Visan T (2016) Electrodeposition of Co and CoMo alloys coatings using choline chloride based ionic liquids—Evaluation of corrosion behaviour. *Trans IMF* 93:302–312. <https://doi.org/10.1080/00202967.2015.1117262>
40. Yang PX, An MZ, Su CN, Wang FP (2008) Fabrication of cobalt nanowires from mixture of 1-ethyl-3-methylimidazolium chloride ionic liquid and ethylene glycol using porous anodic alumina template. *Electrochim Acta* 54:763–767. <https://doi.org/10.1016/j.electacta.2008.06.064>

41. Richard T, Carlin PC, Trulove Hugh C, Long De (1996) Electrodeposition of cobalt-aluminum alloys from room temperature chloroaluminate molten salt. *J Electrochem Soc* 143(9):2747
42. Yang YJ, Zhao GJ, Hu S (2007) Direct current electrodeposition of carbon nanofibers in DMF. *Electrochem Commun* 9:2681–2685. <https://doi.org/10.1016/j.elecom.2007.08.021>
43. Ebadi M, Basirun WJ, Alias Y, Mahmoudian MR, Leng SY (2012) Investigation of electrodeposition of Ni–Co–Fe–Zn alloys in DMSO with MHD effect. *Mater Charact* 66:46–55. <https://doi.org/10.1016/j.matchar.2012.01.011>
44. Barati Darband G, Aliofkhaezrai M, Rouhaghdam AS (2019) Facile electrodeposition of ternary Ni–Fe–Co alloy nanostructure as a binder free, cost-effective and durable electrocatalyst for high-performance overall water splitting. *J Colloid Interface Sci* 547:407–420. <https://doi.org/10.1016/j.jcis.2019.03.098>
45. Sanches LS, Domingues SH, Carubelli A, Mascaro LH (2003) Electrodeposition of Ni–Mo and Fe–Mo alloys from sulfate-citrate acid solutions. *J Braz Chem Soc* 14(4):556–563. <https://doi.org/10.1590/S0103-50532003000400011>
46. Li WR, Hao JJ, Liu W, Mu SH (2021) Electrodeposition of nano Ni–Co alloy with (220) preferred orientation from choline chloride-urea: Electrochemical behavior and nucleation mechanism. *J Alloys Compd* 853:157158. <https://doi.org/10.1016/j.jallcom.2020.157158>
47. Li WR, Hao JJ, Mu SH, Liu W (2020) Electrochemical behavior and electrodeposition of Ni–Co alloy from choline chloride-ethylene glycol deep eutectic solvent. *Appl Surf Sci* 507:144889. <https://doi.org/10.1016/j.apsusc.2019.144889>
48. Scharifker B, Hills G (1982) Theoretical and experimental studies of multiple nucleation. *Electrochim Acta* 28(7):879–889. [https://doi.org/10.1016/0013-4686\(83\)85163-9](https://doi.org/10.1016/0013-4686(83)85163-9)
49. Abu-Zied BM, Soliman SA, Asiri AM (2019) Role of rubidium promotion on the nitrous oxide decomposition activity of nanocrystalline Co_3O_4 - CeO_2 catalyst. *Appl Surf Sci* 479:148–157. <https://doi.org/10.1016/j.apsusc.2019.01.200>
50. Winiarski J, Tylus W, Winiarska K, Szczygieł B (2015) The influence of molybdenum on the corrosion resistance of ternary Zn–Co–Mo alloy coatings deposited from citrate–sulphate bath. *Corros Sci* 91:330–340. <https://doi.org/10.1016/j.apcata.2013.05.011>
51. Clayton CYLRC (1989) An XPS study of the passive and transpassive behavior of molybdenum in deaerated 0.1 M HCl. *Corros Sci* 29:927–937
52. Zhang K, Liu CL, Graham N, Zhang G, Yu WZ (2021) Modulation of dual centers on cobalt-molybdenum oxides featuring synergistic effect of intermediate activation and radical mediator for electrocatalytic urea splitting. *Nano Energy* 87:106217. <https://doi.org/10.1016/j.nanoen.2021.106217>
53. Maity S, Singh DK, Bhutani D, Prasad S, Waghmare UV, Sampath S et al (2021) High surface area NiCoP nanostructure as efficient water splitting electrocatalyst for the oxygen evolution reaction. *Mater Res Bull* 140:111312. <https://doi.org/10.1016/j.materresbull.2021.111312>
54. Gao D, Guo JN, Cui X, Yang L, Yang Y, He HC, Xiao P, Zhang YH (2017) Three-dimensional dendritic structures of NiCoMo as efficient electrocatalysts for the hydrogen evolution reaction. *ACS Appl Mater Interfaces*. <https://doi.org/10.1021/acsami.7b04009>
55. Fricoteaux P, Rousse C (2008) Influence of substrate, pH and magnetic field onto composition and current efficiency of electrodeposited Ni–Fe alloys. *J Electroanal Chem* 612(1):9–14. <https://doi.org/10.1016/j.jelechem.2007.08.022>
56. Wu YH, He HW (2018) Direct-current electrodeposition of Ni–S–Fe alloy for hydrogen evolution reaction in alkaline solution. *Int J Hydrogen Energy* 43:1989–1997. <https://doi.org/10.1016/j.ijhydene.2017.12.015>
57. Kibsgaard J, Jaramillo TF (2014) Molybdenum phosphosulfide: an active, acid-stable, earth-abundant catalyst for the hydrogen evolution reaction. *Angew Chem Int E* 53:14433–14437. <https://doi.org/10.1002/anie.201408222>

Publisher's Note Springer Nature remains neutral with regard to jurisdictional claims in published maps and institutional affiliations.

Springer Nature or its licensor (e.g. a society or other partner) holds exclusive rights to this article under a publishing agreement with the author(s) or other rightsholder(s); author self-archiving of the accepted manuscript version of this article is solely governed by the terms of such publishing agreement and applicable law.